

# Monopole Cavity Resonator Antenna with AMC and Superstrate for 5G/WiMAX Applications

Akhilesh Verma,<sup>#</sup> Ravi Kumar Arya<sup>§,\*</sup> and Srinivasa Nallanthighal Raghava<sup>%</sup>

<sup>#</sup>*Bhumi Entech Equipments Pvt., Ltd., Delhi – 110 075, India*

<sup>§</sup>*Zhongshan Institute of Changchun University of Science and Technology, Zhongshan, Guangdong, China*

<sup>%</sup>*Delhi Technological University, Delhi – 110 042, India*

<sup>\*</sup>*E-mail: raviarya@gmail.com*

## ABSTRACT

For 5G and WiMAX applications, a coplanar waveguide (CPW)-fed monopole antenna sandwiched between an artificial magnetic conductor (AMC) and a superstrate is investigated. Because traditional planar antennas have low gains, they are unsuitable for a wide range of applications. This paper explores scientific strategies for increasing radiation gain in low-gain antennas such as planar monopoles. We use AMC in conjunction with superstrate to achieve a high gain antenna, with the monopole antenna serving as the primary radiator. However, a superstrate like this demands the use of materials with high permittivity, and most of such materials are not readily available on the market. Even if such materials are available, they are mostly expensive and unsuitable for commercial systems. We investigate various superstrates and elaborate on which way these superstrates can be used interchangeably without compromising antenna performance. In the end, we fabricate one of these three superstrates. The antenna, which also employs AMC in tandem with the superstrate, has an impedance bandwidth ranging from 3.2 GHz to 3.75 GHz with 7 dBi gain, so it can be a viable candidate for 5G and WiMAX applications.

**Keywords:** Monopole antenna; Metasurface superstrate; High gain

## 1. INTRODUCTION

Because of their simple structure, short length, economical design, and omnidirectional radiation pattern, monopole antennas are employed in wireless communication.<sup>1</sup> Fifth-generation (5G) technology requires antennas that have high-speed data transmission rates, are compact, and have a high gain for a wide coverage of the network. The 5G technology is the next advanced wireless technology with a high-speed data rate, low latency, and more coverage as compared to all previous existing technologies like 1G to 4G.<sup>2-3</sup> The monopole antenna's omnidirectional design is advantageous for 5G communication.<sup>4-5</sup> If the size of the antenna reduces, its directivity also decreases.<sup>6</sup> As a result, there is a need to improve the monopole antenna's radiation qualities.

The research work<sup>7</sup> suggested a dual-band, dual-sleeve monopole antenna with frequency band coverage of 900 MHz and 1800 MHz. The research work<sup>8</sup> described a crinkle fractal monopole antenna for multiband applications. As described in the research work,<sup>9</sup> a sleeve addition to the monopole antenna enhances its gain to 3.9 dBi. The research work<sup>10</sup> describes a tiny, flexible anisotropic metamaterial coating with an increased radiation gain of up to 5.46 dBi and broader bandwidth (2.15–4.6 GHz). The research work<sup>11</sup> presented a polarization-reconfigurable monopole antenna with a maximum radiation gain of 1.2 dBi that achieves LHCP/RHCP utilising two PIN diodes. Furthermore, an AMC addition can improve the antenna's radiation gain and performance. The

research works<sup>12-13</sup> showed a vertically polarised, omnidirectional, and low-profile antenna with a 5.5% bandwidth and 3.7 dBi gain. The research work<sup>14</sup> describes a low-profile vertical monopole device with a conventional metallic reflector plane. The research work<sup>15</sup> reports a double-printed crossing dipole pair employing vacant quarter-rings, where the back radiation reduces after using square AMC.

The antenna<sup>16</sup> consists of a low-profile vertically polarised monopole antenna and a horizontally polarised circular loop antenna. For a 45% impedance bandwidth and a steady radiation pattern within the band, this design used an AMC that functions as a reflector instead of a Perfect Electric Conductor (PEC). Another antenna design<sup>17</sup> uses a square shape AMC and shows a maximum gain of 6 dBi. There are also several gain improvement strategies using dielectric superstrate. The use of a dielectric superstrate to improve radiation gain was reported in<sup>18-20</sup> addressed the gain increase in a microstrip patch antenna utilizing a dielectric superstrate.

This paper discusses the design of a low-profile CPW-fed monopole antenna sandwiched between an AMC and a superstrate. To comprehend the design, we must first discuss the AMC design and its performance. After the AMC design is finalized, the superstrate design is created. We employ three alternative superstrate configurations for the superstrate design. Next, we examine all three superstrates and investigate how these superstrates can be utilized interchangeably without compromising antenna performance. Finally, one of the superstrates is used to fabricate the proposed antenna, which is then characterized by measuring S-parameters and far-field radiation patterns. Electromagnetic simulations were carried out using ANSYS HFSS.

**2. PROPOSED ANTENNA DESIGN**

Figure 1(a) shows a standard antenna with an AMC on one side and the superstrate on the other. Radiations from the antenna are reflected from the AMC and then reradiated via the superstrate as a result of the Fabry-Perot phenomenon<sup>21-22</sup>. The combined impact of AMC and superstrate results in a high-gain antenna if the design characteristics are well-chosen.

**2.1 Monopole Design**

Figure 1(b) depicts the utilization of a monopole antenna fed by CPW as the radiating element with FR4 substrate

( $\epsilon_r=4.4$ ,  $\tan\delta=0.02$ ). At a frequency of 3.5 GHz, the monopole antenna length is roughly  $\lambda_g/4$ . The antenna's other dimensions are as follows:  $h_m=17$  mm;  $w=3.2$  mm;  $c=9.1$  mm;  $n=0.3$  mm;  $l_3=10$  mm; and  $t_2=1.6$  mm.

**2.2 AMC Design**

The AMC central frequency is chosen first, followed by the AMC design. Our design's AMC central frequency is 3.5 GHz. A 10 mm by 10 mm unit cell is employed as an artificial magnetic conductor. Following that, a square-shaped pixel of side,  $a$ , is placed in the middle of the grounded substrate (FR4)

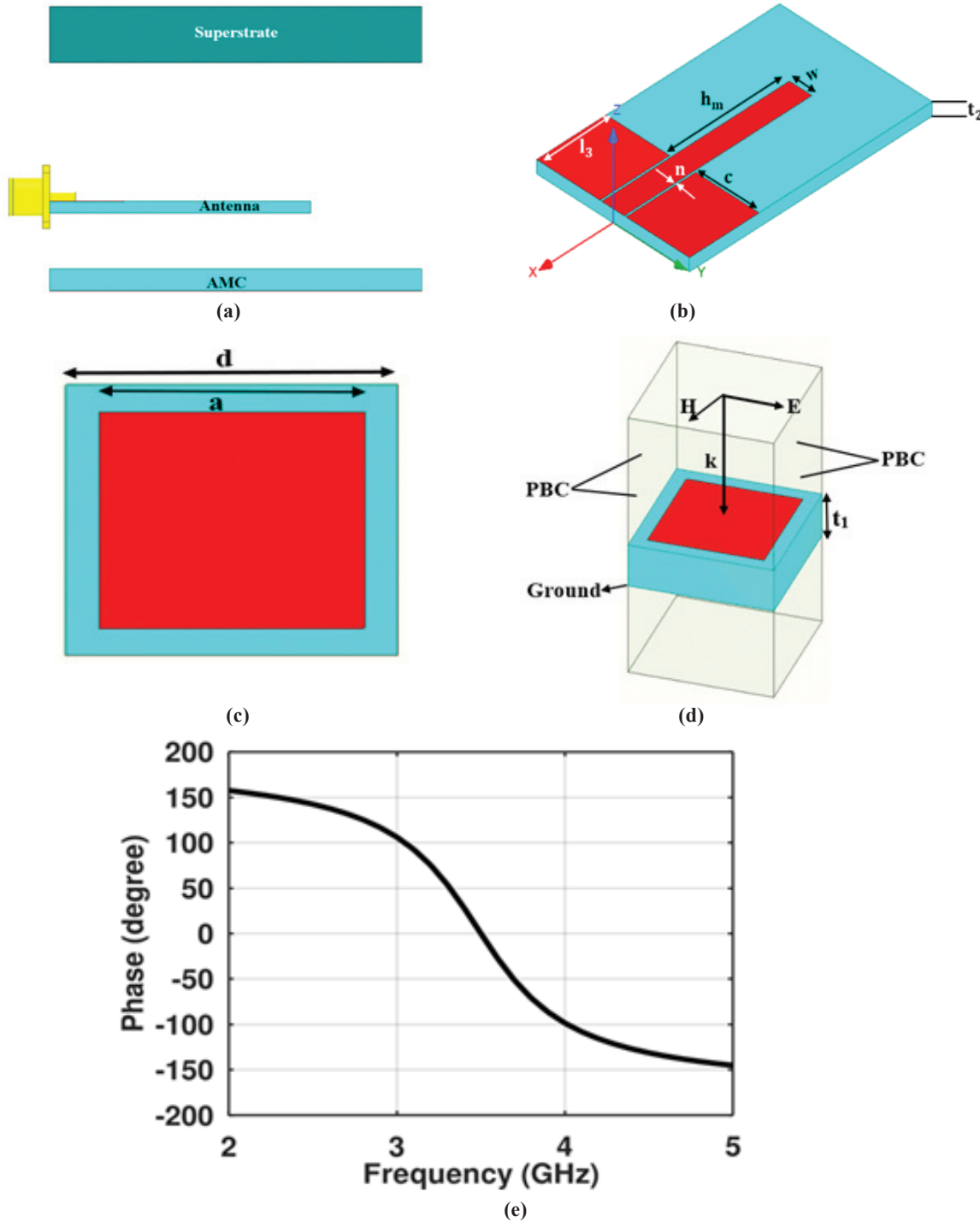


Figure 1. (a) Conventional antenna with AMC and superstrate, (b) Monopole antenna; Unit cell views: (c) Top, (d) Isometric and (e) Reflection behavior.

of the thickness ( $t_1$ ) 3.2 mm, as shown in Fig. 1(c). Figure 1(d) shows a unit cell with boundary conditions, which in this case are periodic. The reflection phase and magnitude are then determined using the Floquet port for simulation purposes.

The pixel side,  $a$ , is then changed such that we get a reflection phase of zero degrees at the target frequency of 3.5 GHz. Figure 1(e) demonstrates that when the pixel's side,  $a$ , is 9.58 mm, the reflection phase approaches zero degrees.

In terms of reflection, AMC has a benefit over PEC in that AMC may be placed extremely close to a transmitting antenna to improve forward radiation. As shown in Fig. 2, we

situate AMC in our design so that AMC touches the dielectric of the CPW-fed monopole antenna. 5×5 AMC cells are used to restrict antenna real estate to a minimum.

For better impedance matching for the radiator, AMC is frequently situated away from it. However, if AMC is not placed away from the antenna, it has the potential to damage the entire antenna system. In normal circumstances, the foam maintains the separation space between the AMC and the radiating element, which must be kept in good condition. We avoid this problem in our design by moving the AMC closer such that there is no space between it and the radiating antenna.

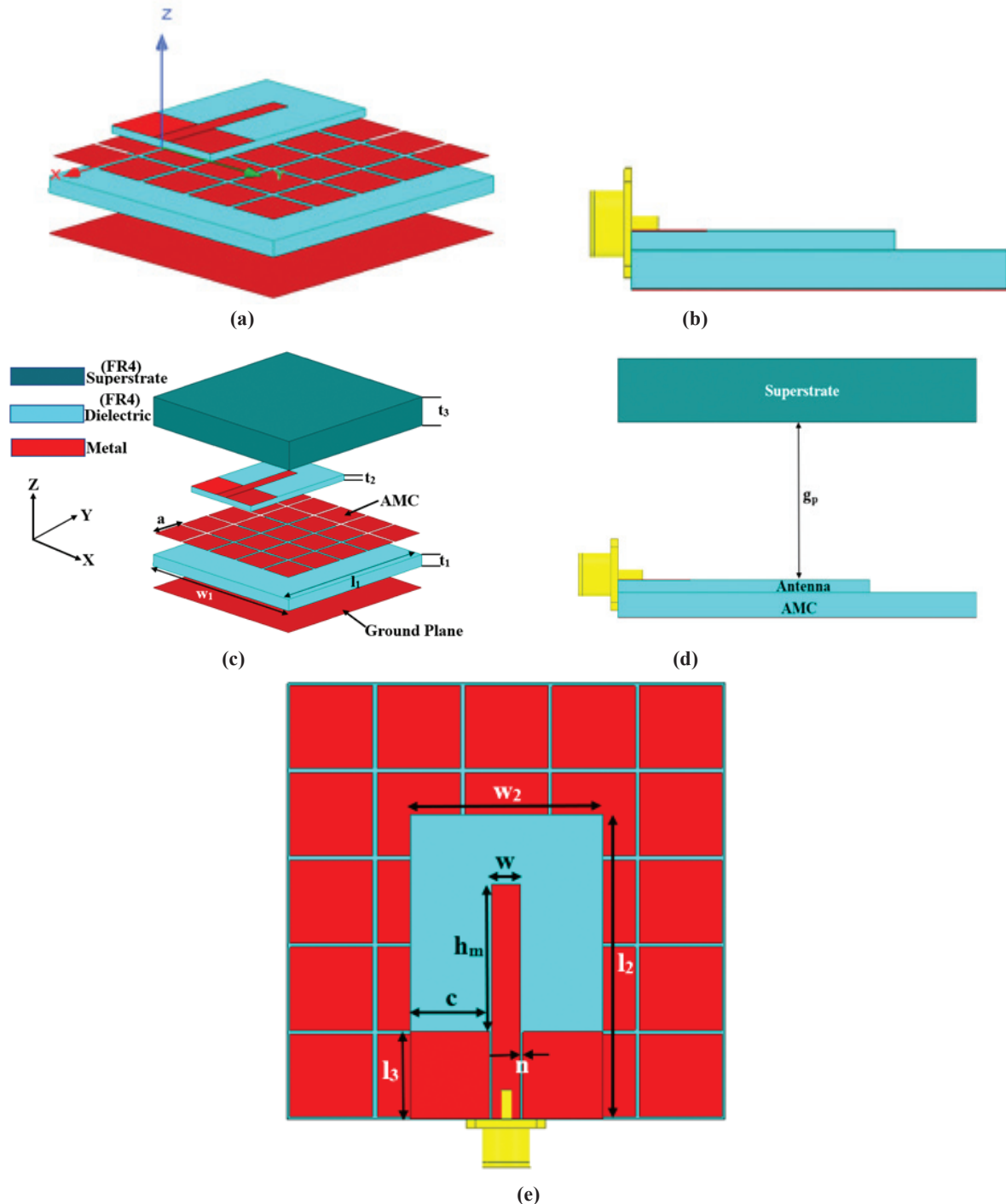


Figure 2. Monopole antenna with AMC: (a) Exploded view, (b) Side view; Geometry of the proposed low permittivity dielectric superstrate antenna, (c) Exploded view, (d) Side view, and (e) Top view.

As a result, the composite antenna structure is stronger and more long-lasting.

Figure 2(c) depicts the low permittivity superstrate designed antenna. The monopole antenna in this arrangement is printed on an FR4 substrate with the following dimensions:  $l_2$ (30mm),  $w_2$ (22mm), and  $t_2$  (1.6mm). The antenna has a rectangular form with dimensions of  $h_m \times w$  and is fed by a CPW with dimensions of  $c(9.1\text{mm}) \times l_3(10\text{mm})$ . As previously mentioned, the proposed antenna is mounted on the AMC.

Figure 3 shows the S-parameters and gain (at  $\theta=0$ ,  $\Phi=0$ ) for monopole antennas in the presence or absence of AMC to demonstrate the AMC significance. Such results ascertain that AMC usage reduces bandwidth while increasing composite structure gain. As a result of AMC loading the antenna, the impedance bandwidth decreases. Figure 3(b) shows that using AMC increases the antenna gain by more than 5 dBi. It is also worth noting that after applying AMC and or superstrate, the resonance frequency shifts from 3.3 GHz to 3.5 GHz.

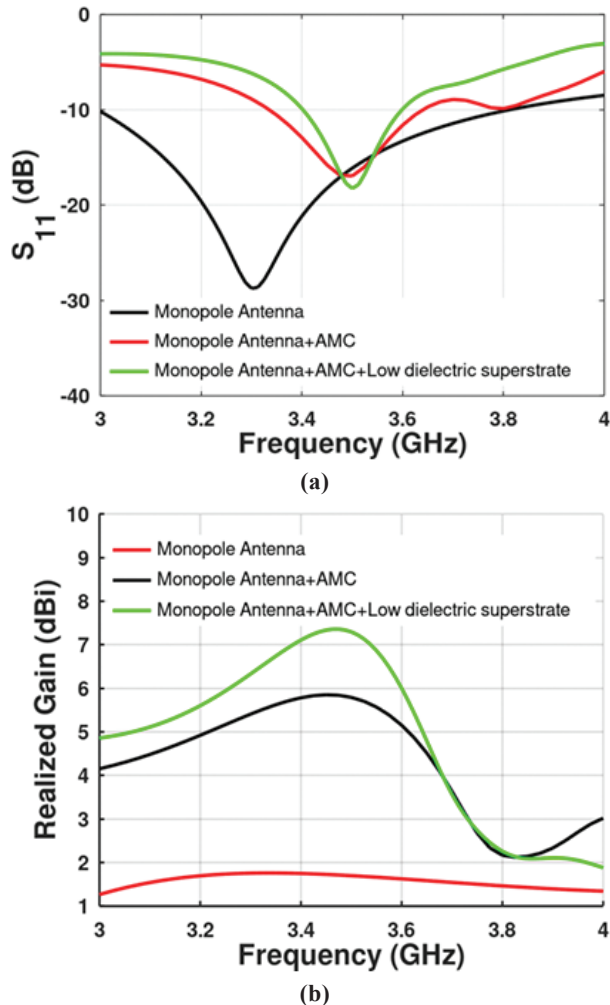


Figure 3. (a) Simulated realized gain, and (b) S-parameters.

### 3. DESIGN AND ANALYSIS OF SUPERSTRATES

We start with the AMC before going on to the superstrate design. In the current work, we provide three superstrate architectures with interchangeable parts and comparable functionalities. Three designs were established to give designers more options and avoid them being compelled to rely just on

one superstrate design technique. It also allows designers to choose the most cost-effective superstrate.

As we will show later, due to their design, two such substrates can also be fabricated by 3D-printing techniques directly without using time-consuming PCB etching.<sup>23-25</sup>

The superstrate's transmission and reflection behaviors determine the antenna's overall gain and aid in producing a cavity effect similar to the Fabry-Perot phenomenon.<sup>21-22</sup> AMC and superstrate are used to build the cavity on opposite sides.

In this work, three superstrates are made, and their properties are compared to see if they offer similar performance. Similar to how AMC is examined, the metasurface superstrate is also explored. However, in superstrate design, transmission behavior is also investigated.<sup>21-22</sup>

For comparison, we make use of the following superstrates:

#### 3.1 Metasurface Superstrate

In this case, a 1.6mm thick metasurface superstrate (FR4) is used. In the metasurface superstrate, metallic square patches with 7.26 mm sides are placed in a  $5 \times 5$  grid. The distance between the antenna and the metasurface superstrate layer is 21.4 mm, which is equal to  $\lambda/4$ .

#### 3.2 Low Dielectric Superstrate

In this instance, an 8mm thick low dielectric superstrate with a 21.4 mm gap, or  $\lambda/4$ , and a permittivity of 4.4 (FR4) is situated above the antenna.

#### 3.3 High Dielectric Superstrate

A high dielectric substance with a permittivity of 16.1 is required for this superstrate. The 1.6 mm thick high dielectric superstrate is positioned over a 21.4 mm distant antenna. In this case, to increase the antenna's gain, this superstrate needs material with a high dielectric constant of 16.1.

Figures 4(a), (b) and (c) depict all three types of superstrates with a composite of antenna and AMC.

The equivalent dielectric approach, as described in,<sup>23-25</sup> has been used when simulating and analyzing the three superstrate designs. Then, we compare the properties of the superstrates after each one is placed on the antenna. Figure 4(d) compares the  $S_{11}$  of the three superstrate antenna designs. The reflection coefficients of all antennas are virtually identical and resonant at 3.5 GHz, as can be seen in Fig. 4(d). Figure 4(e) shows that the three superstrate antennas' gain is very close to one another too.

The three superstrate design simulations demonstrate that any of the superstrates can be used to enhance the gain of the suggested antenna. The high dielectric superstrate has an expensive and difficult-to-find permittivity value of 16.1, which is a high value. The metasurface superstrate needs  $5 \times 5$  unit cells to increase the antenna's gain. With a permittivity of 4.4 and an 8 mm thickness, the low dielectric superstrate antenna attains the same gain as the metasurface and high dielectric superstrate antennas. We demonstrate the following alternative methodologies for study to get insights into how the three superstrates share comparable features.<sup>21-22</sup>

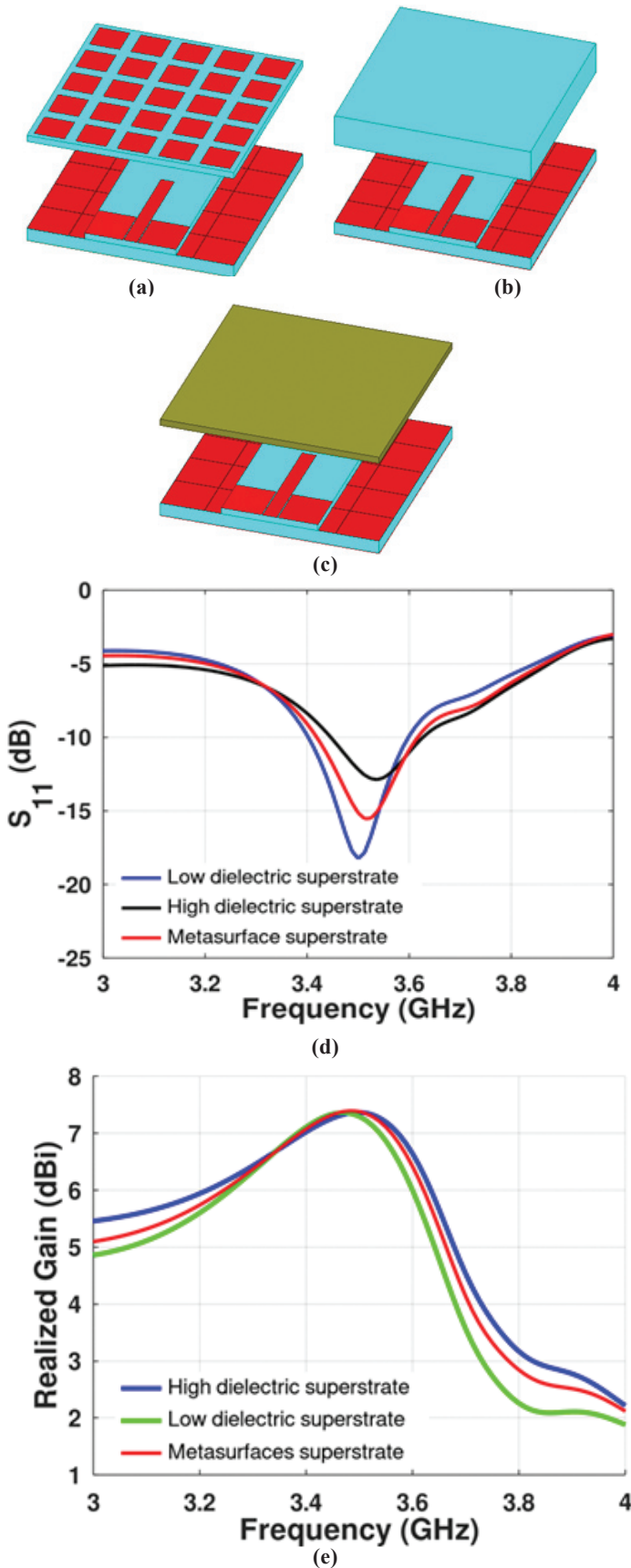


Figure 4. Different antennas: (a) Metasurface superstrate, (b) Low dielectric superstrate, (c) High dielectric superstrate, (d)  $S_{11}$  of the three superstrate antennas, and (e) Simulated gain of the three superstrate antennas.

#### 4. TRANSMISSION/REFLECTION ANALYSIS OF SUPERSTRATES

For each of the three superstrates, we produce periodic unit cells and examine them independently.<sup>24</sup> A unit cell with the dimensions  $10 \text{ mm} \times 10 \text{ mm}$  is used for this analysis. The reflection and transmission behavior of unit cells in three superstrates is depicted in Fig. 5. This study reveals that the reflection and transmission properties of all the superstrates are comparable. To obtain equivalent radiation characteristics from the antenna, they can be swapped out for one another if their reflection/transmission response is the same.

We also examine the near-field characteristics of the different antennas to verify the effectiveness of the superstrate.

To do a near-field study, we draw a horizontal line in the center of the antenna and research as described in.<sup>23</sup> For this investigation, a line above the superstrate is used to collect and analyze the dominating electric field (in this example,  $E_x$ ). The field measurement line is positioned 1 mm above the superstrate. In other words, a field with a uniform phase will produce constructive interference, producing more gain with the superstrate. The superstrate should produce uniform fields above the superstrate. Figures 6(a) and (b) display the magnitude and phase values of the dominant  $E_x$  field on the line. The phase is straightened when a superstrate is present as can be seen from the phase plot. It implies that the near field will contribute positively, which results in a higher gain. When the measurement plane rather than a line is employed to measure the near fields, as shown in Figures 6(c-f), similar behavior is observed. The phase lines of Fig. 6(b), (d) and (f) are straight, indicating that the addition of superstrate has corrected the phase, causing the radiating field to converge and thus increase in gain.

We create a thick dielectric superstrate out of the three superstrate antenna options to see how well the simulation results match the measurements of the built antenna.

#### 5. PARAMETRIC STUDIES OF THE PROPOSED ANTENNA

To determine the antenna's optimal dimensions, parametric variation research is carried out. The suggested low dielectric superstrate antenna's performance is compared by changing  $g_p$  between the superstrate and the antenna. Figure 5 depicts the antenna's  $S_{11}$  performance by a change in  $g_p$ . The optimal value of  $g_p$  is selected to be 21.4 mm for the specified center frequency and bandwidth.

#### 6. SIMULATIONS AND MEASUREMENT RESULTS

The fabricated antenna as shown in Fig. 8(a) is measured using the R & S Vector Network Analyzer (up to 40GHz) and anechoic chamber.

##### 6.1 S-parameters

The parametric variation research is conducted to determine the antenna's optimal dimensions. The suggested low dielectric superstrate antenna's performance is compared by changing  $g_p$  between the superstrate and antenna. Figure 5 depicts the antenna's  $S_{11}$  performance by a change in  $g_p$ . The optimal value of  $g_p$  is selected to be 21.4 mm for the specified center frequency and bandwidth.

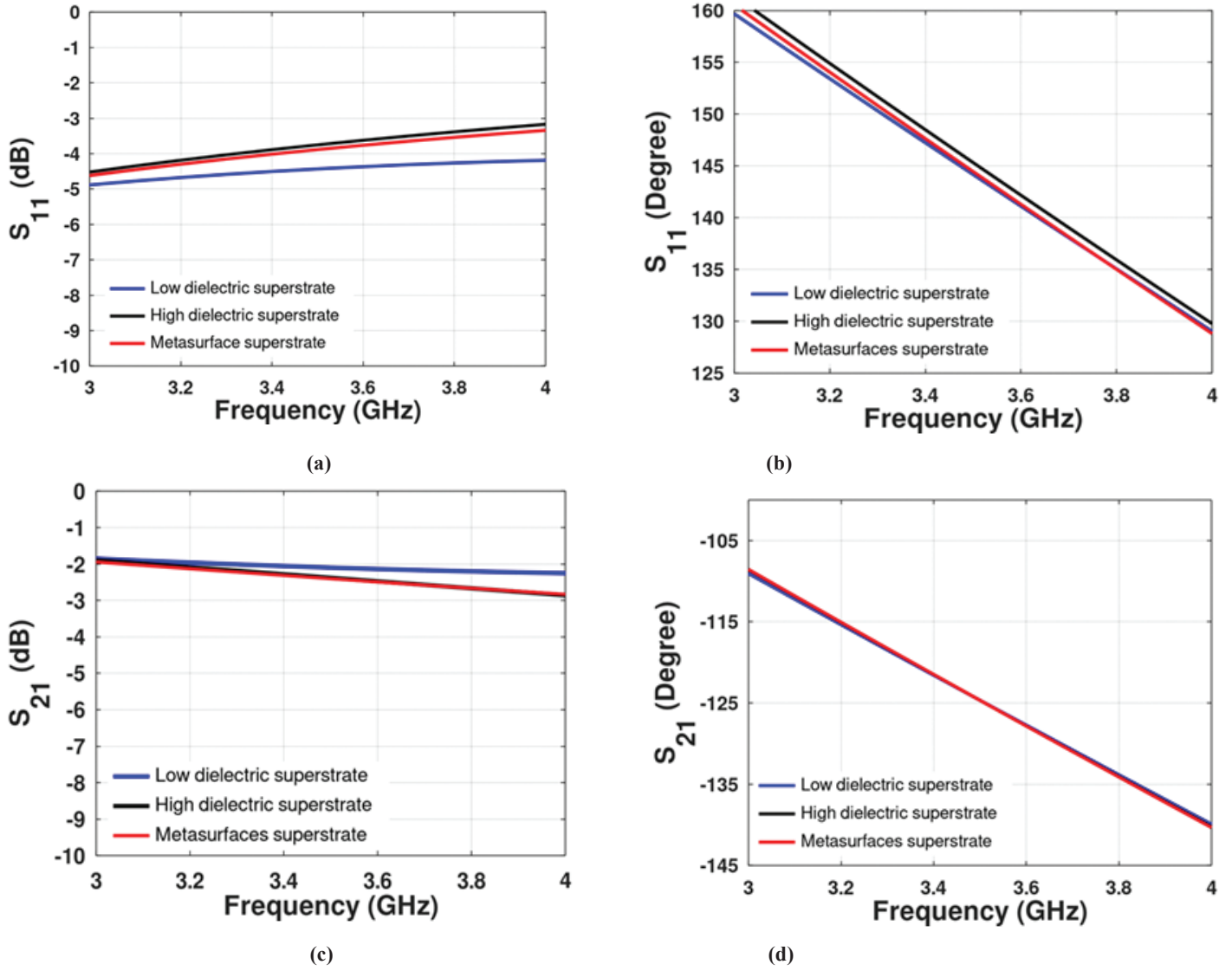


Figure 5. Simulated reflection and transmission behavior: (a)  $S_{11}$  magnitude, (b)  $S_{11}$  phase, (c)  $S_{21}$  magnitude, and (d)  $S_{21}$  phase.

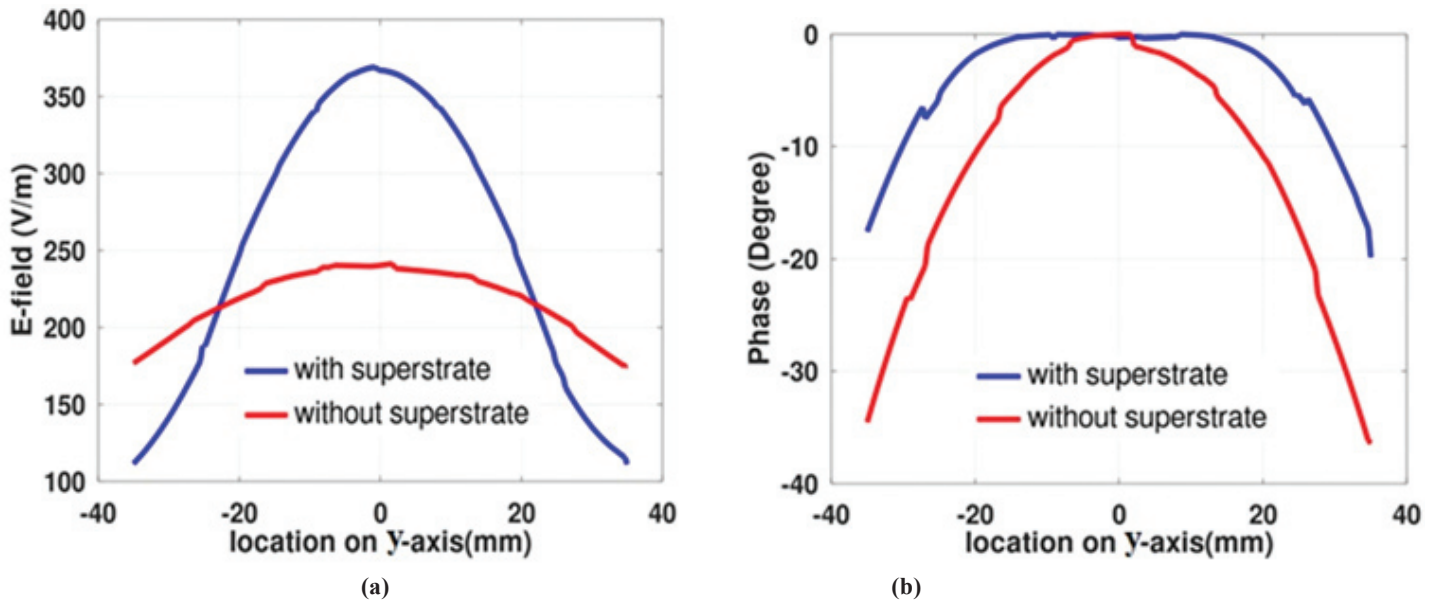


Figure 6(a) Proposed antenna near field performance in terms of E-field magnitude on a line, and (b) phase on a line.

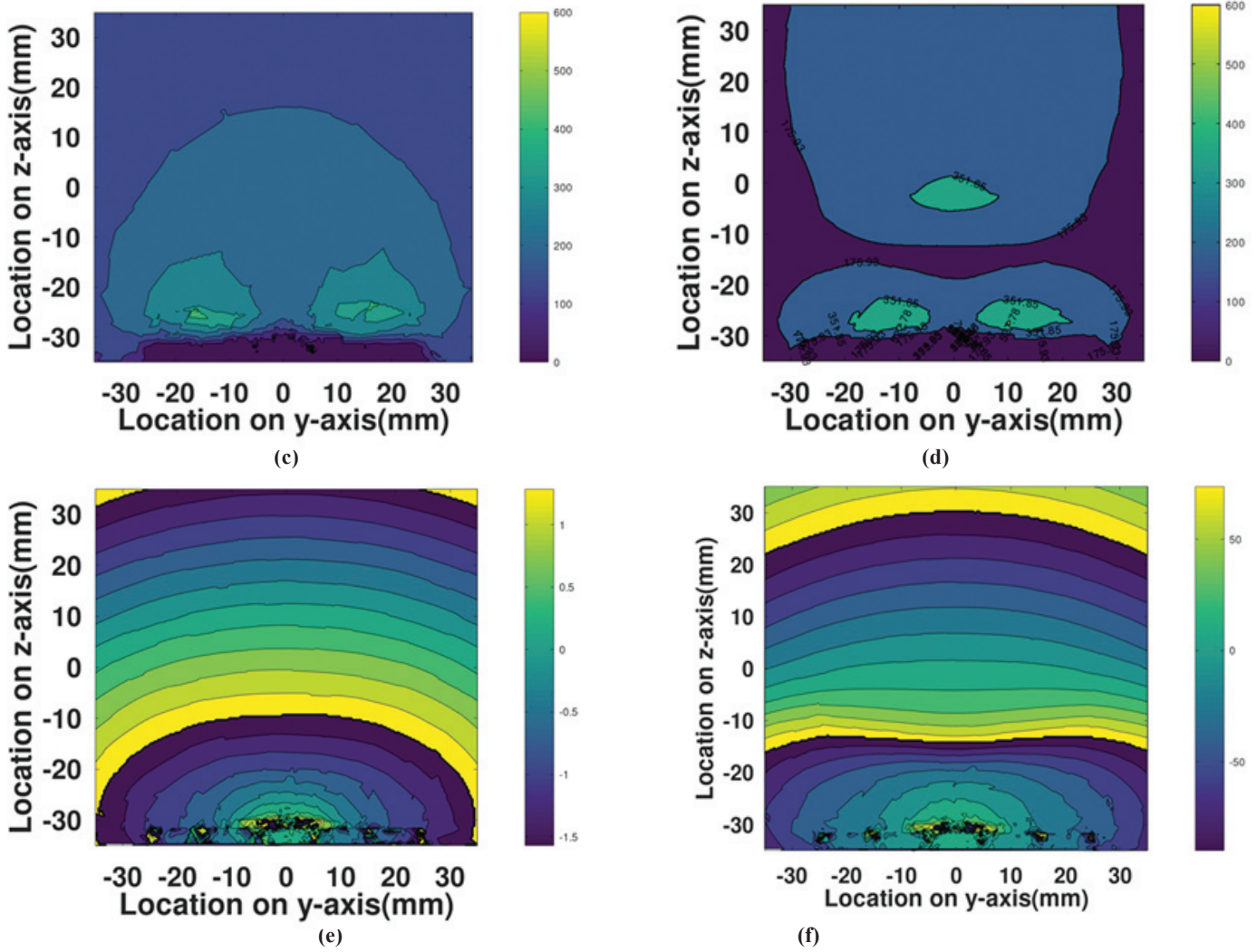


Figure 6(c) Proposed antenna near field performance in terms of E-field magnitude on a plane in absence of superstrate, (d) Magnitude on a plane in presence of superstrate, (e) Phase on a plane in absence of superstrate, and (f) Phase on a plane in presence of superstrate

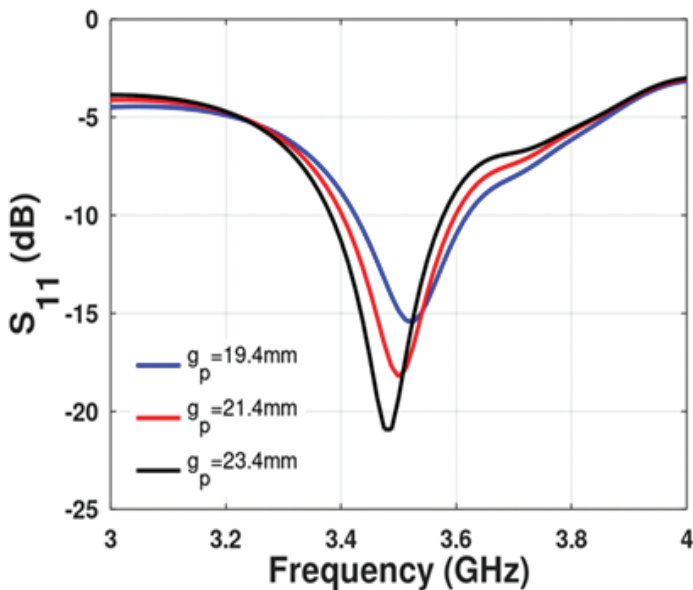


Figure 7. Simulated  $S_{11}$  of the proposed antenna with different  $g_p$ .

### 6.2 Proposed Antenna Radiation Performance

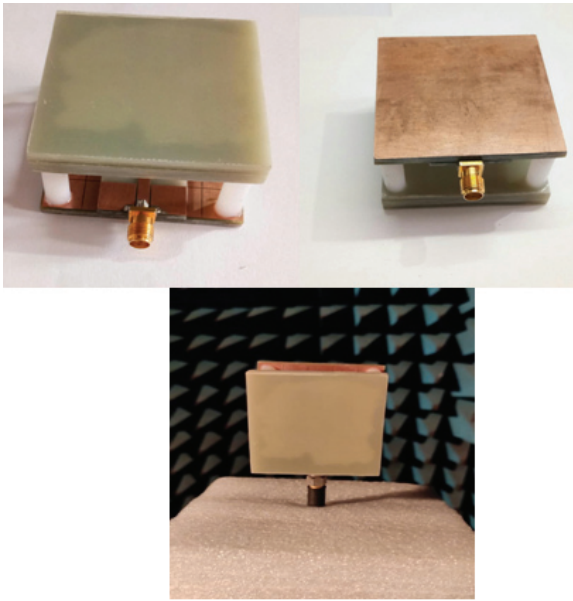
The radiation properties of the antenna are investigated by radiation patterns (3.5 GHz) as depicted in Fig. 9(a) and (b). The co-polarized gain values are shown in red color while the cross-pol gain values by black color. The dashed lines are from measurements while the continuous lines are from simulations. It is evident that the antenna provides improved cross-polarization behavior.

### 6.3 Gain

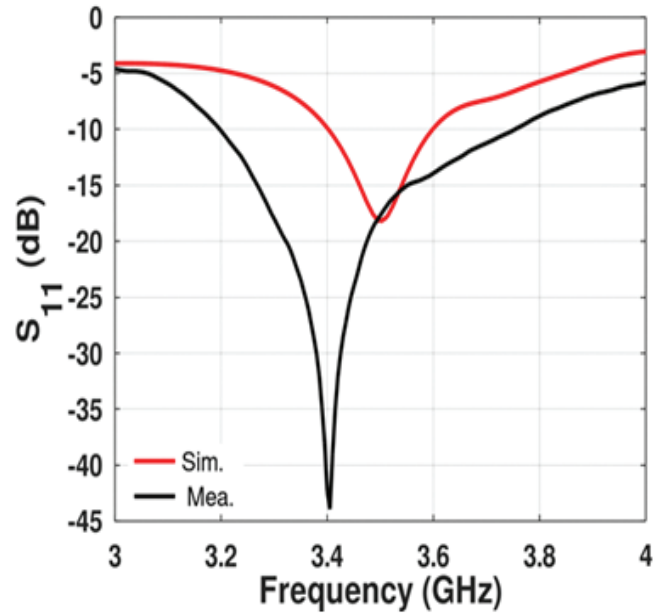
Figure 10 demonstrates that at 3.5 GHz, the gain from simulations and measurements are, respectively, 7.3 dBi and 7 dBi. We discover that the simulated gain closely resembles the measured gain.

### 6.4 Efficiency

Figure 11 displays the proposed antenna's radiation efficiency in both simulated and measured forms. The figure shows that the antenna is moderately efficient. However, utilizing materials with lower losses will boost the antenna efficiency. But, in the current design, FR4 was chosen over more expensive dielectrics with low-loss tangents to keep the antenna's cost low.

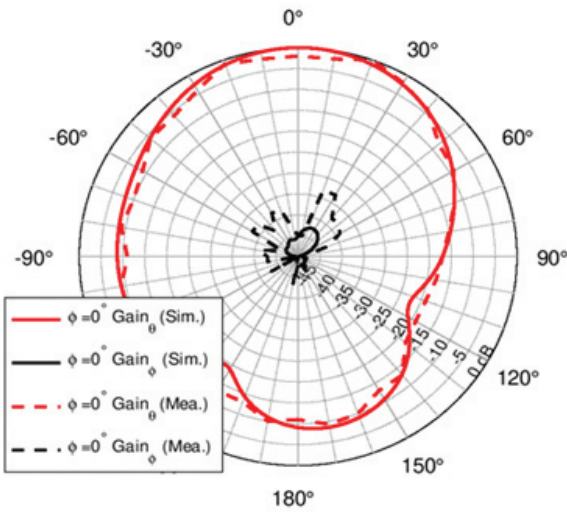


(a)

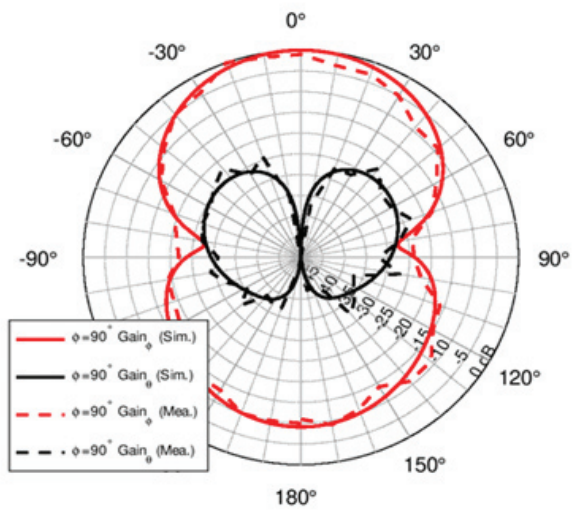


(b)

Figure 8. (a) Fabricated antenna, and (b) Measured and simulated  $S_{11}$



(a)



(b)

Figure 9. Radiation patterns at 3.5 GHz: (a)  $\phi=0^\circ$  cut, and (b)  $\phi=90^\circ$  cut.

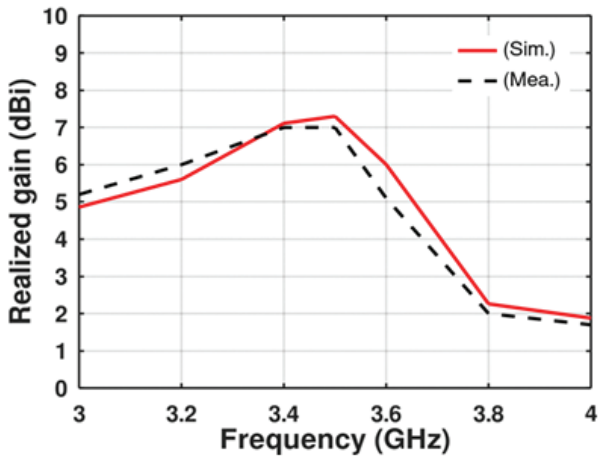


Figure 10. Realized gain of the antenna.

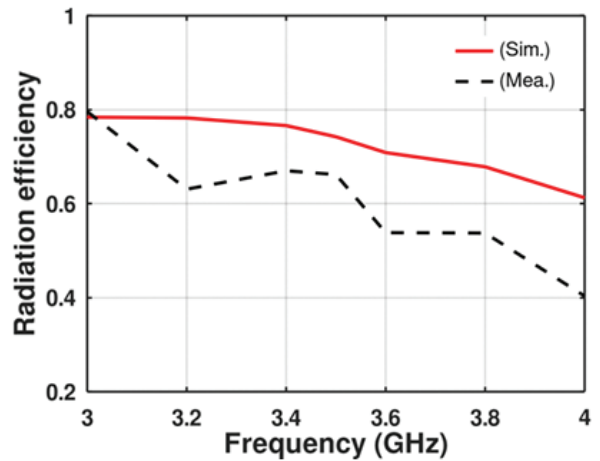


Figure 11: Radiation Efficiency

Table 1 shows the comparison of various antennas from the literature with the proposed antenna. We can observe that the proposed antenna is very competitive in size and has the highest gain when compared to other antennas. These features make this antenna suitable for WiMAX use. If deployed in a MIMO arrangement with similar antennas, it might make a good contender for 5G.

References	Size ( $\lambda^3$ )	BW (GHz)	Gain (dBi)
[9]	$\pi/4 \times 0.82^2 \times 0.24$	2.38–2.54	3.9
[10]	-	2.15–4.6	3.7-5.46
[14]	$0.32 \times 0.32 \times 0.025$	1.98 - 2.08	3.7
[17]	$1.12 \times 1.12 \times 0.09$	4.83–6.25	6
[20]	$4.05 \times 4.05 \times 1.21$	5.71-5.87	6.8
Our Design	$1.22 \times 1.22 \times 0.798$	3.2-3.75	7

## 7. CONCLUSION

This manuscript proposed a method to enhance the radiation gain of the antenna by using AMC and superstrate. The performances of the proposed antenna with three contending superstrates were conducted. In last, a superstrate in the combination with antenna-AMC was manufactured. The proposed antenna covers a 3.2-3.75 GHz band and has a radiation gain of 7 dBi which makes it a suitable candidate for 5G and WiMAX applications.

## REFERENCES

- Deng, C.; Xie, Y.J. and Li, P. CPW-fed planar printed monopole antenna with impedance bandwidth enhanced. *IEEE Antennas Propag. Lett.*, 2009, **8**, 1394-1397. doi: 10.1109/LAWP.2009.2039743
- S. Mondal.; A. Sinha, and J. Routh. A Survey on Evolution of Wireless Generations 0G to 7G, *Int. J. Adv. Res. Sci. Eng.*, 2015, **1**(2), 5–10.
- Bhalla, M.R. & Bhalla, A.V. Generations of mobile wireless technology: A Survey, *Int. J. Comput. Appl.*, 2010, **5**(4), 26–32. doi: 10.5120/905-1282
- Princess, J.P.; Let, G.S.; Rizopackiamary, P. & Keziah, J. Design of Dual-band monopole antenna for mobile communications. In *IEEE 2<sup>nd</sup> International Conference on Signal Processing and Communication (ICSPC)*, 2019, pp. 70-73. doi: 10.1109/ICSPC46172.2019.8976789
- Beigi, P. & Mohammadi, P. A novel small triple-band monopole antenna with a crinkle fractal structure. *AEU-Int. J. Electron. Commun. J. Electron. Commun.*, 2016, **70**(10), 1382–1387. doi: 10.1016/j.aeue.2016.07.013
- Jafargholi, A.; Kamyab, M. & Veysi, M. Artificial magnetic conductor loaded monopole antenna. *IEEE Antennas Propag. Lett.*, 2010, **9**, 211–214. doi: 10.1109/LAWP.2010.2046008
- Tan, W. & Shen, Z. A dual-band dual-sleeve monopole antenna. *IEEE Antennas and Wireless Propag. Lett.*, 2017, **16**, 2951-2954. doi: 10.1109/LAWP.2017.2755042
- Beigi, P. & Mohammadi, P. A novel small triple-band monopole antenna with a crinkle fractal structure. *AEU-Int. J. Electron. Commun.*, 2016, **70**(10), 1382-1387. doi: 10.1016/j.aeue.2016.07.013
- Deng, C.; Lv, X. & Feng, Z. High gain monopole antenna with sleeve ground plane for WLAN applications. *IEEE Antennas and Wireless Propag. Lett.*, 2017, **16**, 2199-2202. doi: 10.1109/LAWP.2017.2705916
- Jiang, Z.H.; Gregory, M.D. & Werner, D.H. A broadband monopole antenna enabled by an ultrathin anisotropic metamaterial coating. *IEEE Antennas and Wireless Propag. Lett.*, 2011, **10**, 1543-1546. doi: 10.1109/LAWP.2011.2180503
- Panahi, A.; Bao, X.L.; Yang, K.; O'Conchubhair, O.; and Ammann, M.J. A simple polarization reconfigurable printed monopole antenna. *IEEE Transc. Antennas Propag.*, 2015, **63**(11), 5129-5134. doi: 10.1109/TAP.2015.2474745
- Koohestani, M.; Zürcher, J.F.; Moreira, A.A. & Skrivervik. A novel, low-profile, vertically-polarized UWB antenna for WBAN. *IEEE Transact. Antennas, and Propag.*, 2014, **62**(4), 1888-1894. doi: 10.1109/TAP.2014.2298886
- Abbasi, N.A. & Langley, R.J. Multiband-integrated antenna/artificial magnetic conductor. *Microw. Antennas. Propag.*, 2011, **5**(6), 711–717. doi: 10.1049/iet-map.2010.0200
- Yuan, T.; Díaz-Rubio, A. & Ouslimani, H.H. New subwavelength profile Monopole-Type antenna. *IEEE Transact. Antennas and Propag.*, 2016, **64**(8), 3347-3352. doi: 10.1109/TAP.2016.2576481
- Lin, J.; Qian, Z.; Cao, W.; Shi, S.; Wang, Q. & Zhong, W. A low-profile dual-band dual-mode and dual-polarized antenna based on AMC. *IEEE Antennas and Wireless Propag. Lett.*, 2017, **16**, 2473-2476. doi: 10.1109/LAWP.2017.2724540
- Wu, J.; Yang, S.; Chen, Y.; Qu, S. & Nie, Z. A low profile dual-polarized wideband omnidirectional antenna based on AMC reflector. *IEEE Transact. Antennas and Propag.*, 2016, **65**(1), 368-374. doi: 10.1109/TAP.2016.2631147
- Cao, Y.F.; Zhang, X.Y. & Mo, T. Low-profile conical-pattern slot antenna with wideband performance using artificial magnetic conductors. *IEEE Transact. Antennas and Propag.*, 2018, **66**(5), 2210-2218. doi: 10.1109/TAP.2018.2809619
- Jackson, D.R. & Alexopoulos, N. Gain enhancement methods for printed circuit antennas. *IEEE Transact. Antennas and Propag.*, 1985, **33**(9), 976–987. doi: 10.1109/TAP.1985.1143709
- Jackson, D.R.; Burghignoli, P.; Lovat, G.; Capolino, F.; Ji, C.; Wilton, D.R. & Oliner, A.A. The fundamental physics of directive beaming at microwave and optical frequencies and the role of leaky waves. *IEEE*, 2011,

- 99(10), 1780–1805.  
doi: 10.1109/JPROC.2010.2103530
20. Kim, J.H.; Ahn, C.H.; and Bang, J.K. Antenna gain enhancement using a holey superstrate. *IEEE Transact. Antennas and Propag.*, 2016, **64**(3), 1164-1167.  
doi: 10.1109/TAP.2016.2518650
21. Mitra, R.; Li, Y.; & Yoo, K. A comparative study of directivity enhancement of microstrip patch antennas using three different superstrates. *Microwave and Optical Technol. Lett.*, 2010, **52**(2), 327-331.  
doi: doi.org/10.1002/mop.24898
22. Li, Y.; Mitra, R.; Zeng, B.; Lu, G.; Li, Z.; Liu, J.; & Chang, D. C. Directivity enhancement of fabry-perot antenna by using a stepped-dielectric slab superstrate. *Microwave and Optical Technol. Lett.*, 2012, **54**(3), 711-715.  
doi: 10.1002/mop.26614
23. Zhang, S.; Arya, R.K.; Whittow, W.G.; Cadman, D.; Mitra, R.; and Vardaxoglou, J.C. Ultra-wideband flat metamaterial GRIN lenses assisted with additive manufacturing technique. *IEEE Transact. Antennas and Propag.*, 2020, **69**(7), 3788-3799.  
doi: 10.1109/TAP.2020.3044586.
24. Arya, R.K.; Zhang, S.; Pandey, S.; Kumar, A.; Vardaxoglou, Y.; Whittow, W.; and Mitra, R. Meta-atoms and artificially engineered materials for antenna applications. *Dev. Antenna Analysis and Design*, 2018, **1**, 351-405.  
doi: 10.1049/SBEW543F\_ch10.
25. Zhang, S.; Arya, R.K.; Pandey, S.; Vardaxoglou, Y.; Whittow, W.; and Mitra, R. 3D-printed planar graded index lenses. *IET Microwaves, Antennas & Propag.*, 2016,

10(13), 1411-1419.  
doi: 10.1049/iet-map.2016.0013.

## CONTRIBUTORS

**Dr Akhilesh Verma** obtained his PhD degree in Electronics and Communication Engineering from the Delhi Technological University, Delhi, India, in 2021. He is currently Sr. Engineer (R&D) with Bhumi Entech Equipments Pvt Ltd, Delhi, India. His current research interests include: Metasurfaces, Artificial Magnetic Conductors (AMC), SIW, RF mixers, power amplifier, lumped & microstrip filter design at Ku band, lumped filter design for RADAR applications, lumped and active antennas for 5G applications.

In the current study, he developed the theory and performed the simulations.

**Dr Ravi Kumar Arya** obtained his PhD degree in Electrical Engineering from the Pennsylvania State University, USA in 2017. He is currently working with Xiangshan Laboratory, Zhongshan Institute of Changchun University of Science and Technology, China. His research interests include RF circuit design, antenna design, lens design, and the analysis of frequency-selective surfaces.

In the current study, he developed as well as verified the theory and design of the antenna.

**Prof. N.S. Raghava** is working as a Professor in Electronics and Communication Engineering Department (HOD) at Delhi Technological University, India. His areas of specialisation are Antenna and propagation, microwave engineering, digital communication, wireless comm., cloud computing, information security.

In the current study, he verified the theory and design of the antenna and supervised the findings of this work.